Article

Cell

Peptidoglycan Production by an Insect-Bacterial Mosaic

DeAnna C. Bublitz,[1] Grayson L. Chadwick,[2] John S. Magyar,[2] Kelsi M. Sandoz,[3] Diane M. Brooks,[1] Stéphane Mesnage,[4] Mark S. Ladinsky,[5] Arkadiy I. Garber,[1] Pamela J. Bjorkman,[5] Victoria J. Orphan,[2] and John P. McCutcheon[1,6,*]

[1]Division of Biological Sciences, University of Montana, Missoula, MT 59812, USA
[2]Division of Geological and Planetary Sciences, California Institute of Technology, Pasadena, CA 91125, USA
[3]Coxiella Pathogenesis Section, Laboratory of Bacteriology, Rocky Mountain Laboratories, National Institute of Allergy and Infectious Diseases, NIH, Hamilton, MT 59840, USA
[4]Department of Molecular Biology and Biotechnology, University of Sheffield, Sheffield S10 2TN, UK
[5]Division of Biology and Biological Engineering, California Institute of Technology, Pasadena, CA 91125, USA
[6]Lead Contact
*Correspondence: john.mccutcheon@umontana.edu
https://doi.org/10.1016/j.cell.2019.08.054

SUMMARY

Peptidoglycan (PG) is a defining feature of bacteria, involved in cell division, shape, and integrity. We previously reported that several genes related to PG biosynthesis were horizontally transferred from bacteria to the nuclear genome of mealybugs. Mealybugs are notable for containing a nested bacteria-within-bacterium endosymbiotic structure in specialized insect cells, where one bacterium, *Moranella*, lives in the cytoplasm of another bacterium, *Tremblaya*. Here we show that horizontally transferred genes on the mealybug genome work together with genes retained on the *Moranella* genome to produce a PG layer exclusively at the *Moranella* cell periphery. Furthermore, we show that an insect protein encoded by a horizontally transferred gene of bacterial origin is transported into the *Moranella* cytoplasm. These results provide a striking parallel to the genetic and biochemical mosaicism found in organelles, and prove that multiple horizontally transferred genes can become integrated into a functional pathway distributed between animal and bacterial endosymbiont genomes.

INTRODUCTION

Horizontal gene transfer (HGT) occurs when a gene is moved from the genome of one organism to another outside of the normal processes of vertical inheritance. HGT can, in principle, occur between any two DNA-based life-forms, but most often involves either movement of genes between microorganisms (Koonin et al., 2001; Ochman et al., 2000; Richards et al., 2011) or from microorganisms to larger eukaryotic hosts (Dunning Hotopp, 2011; Husnik and McCutcheon, 2018). The process of HGT in the evolution of the cellular organelles derived from bacteria—the mitochondrion and the plastid—is not disputed and is often referred to as endosymbiont gene transfer (EGT) when the transferred genes seem to originate from the ancestral organelle genome (Keeling and Palmer, 2008; Martin et al., 2002; Timmis et al., 2004). The role that HGT (that is, transfer from sources other than ancestral organelle genomes) has played in the evolution of organelles is less clear, but numerous examples of HGTs from bacteria unrelated to the mitochondrial or plastid ancestor are found in eukaryotic genomes (Gray, 2015; Ku et al., 2015). No matter their genome of origin, the proteins that are produced from these EGTs and HGTs, and that function in organelles are transported there by specific multiprotein complexes (Neupert and Herrmann, 2007; Schleiff and Soll, 2000). This history of gene loss on organelle genomes and gene gain on nuclear genomes has led to complex mosaic biochemical pathways in organelles, where genes of diverse taxonomic origin reside on different genomes, and the protein products of these genes are shuttled to different parts of the cell without strict deference to their taxonomic origins (Duchêne et al., 2005; Gabaldón, 2018; Kořený et al., 2013).

Eukaryotic genome sequencing has led to the discovery of many potential HGT candidates unrelated to organelle function, most often originating from bacterial and fungal sources (Dunning Hotopp and Estes, 2014; Milner et al., 2019; Moran and Jarvik, 2010; Schönknecht et al., 2013; Slot and Rokas, 2011). The roles of these HGTs are diverse, but most often include nutrition or protection from predators, pathogens, and environmental stress (Husnik and McCutcheon, 2018). The function of some of these HGTs has been verified (Chou et al., 2015; Dean et al., 2018; Kominek et al., 2019; Metcalf et al., 2014; Milner et al., 2019; Moran and Jarvik, 2010; Stairs et al., 2018), but these examples all involve single-step biochemical processes or functions gained through the transfer of multiple genes linked by residence on the same fragment of transferred DNA. These functionally verified HGT events serve as important milestones in HGT research, but none approach the complex cellular and biochemical mosaicism observed in some organelle biochemical pathways that result from EGT and HGT.

Genomic work on sap-feeding insects and their nutritional endosymbiotic bacteria has revealed a few cases where the complexity of bacterial integration into host cells seems to approach that of organelles (McCutcheon, 2016; McCutcheon and Moran, 2011; Moran and Bennett, 2014). These bacteria

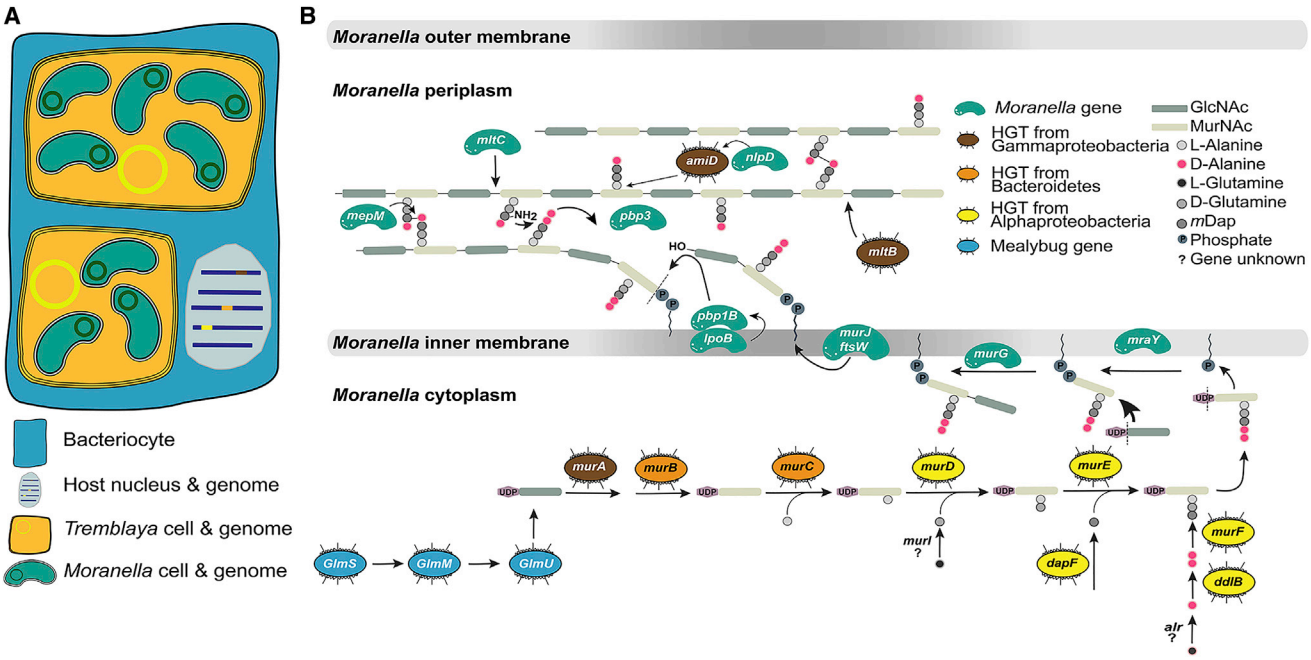

Figure 1. A Complete PG Biosynthesis Pathway Is Predicted by Genomics

(A) Schematic representation of a single *P. citri* bacteriocyte (blue), where *Moranella* cells and their two lipid bilayers (green) reside inside of triple-membrane-bound *Tremblaya* cells (yellow).

(B) Adapted from Typas et al., 2011. A pictorial representation of the genes present and expressed on the genomes of *P. citri* (blue represents native eukaryotic genes, brown represents HGTs of Gammaproteobacteria origin, orange represents HGTs of Bacteroidetes origin, and yellow represents Alphaproteobacteria origin) and *Moranella* (green) that are involved in PG production. The locations of the small colored cell schematics labeled with gene names are based on the predicted location of the protein product of that gene.

See also Table S1.

provide essential nutrients to their hosts and are thus required for normal host biology and survival (Akman Gündüz and Douglas, 2009; Baumann, 2005). Many of these endosymbionts are also long-term associates of their hosts, often living exclusively in special insect cells for tens or hundreds of millions of years (Moran et al., 2005). Like organelles, they are also faithfully transmitted from one host generation to the next by maternal transmission (Koga et al., 2012). This strict host association has resulted in extreme levels of gene loss and genome reduction in some endosymbionts, leading to bacterial genomes that are similar to organelle genomes in terms of gene number and genome size (McCutcheon and Moran, 2011; Moran and Bennett, 2014). In a final parallel to organelle evolution, some of the insects harboring endosymbionts with tiny genomes appear to use both native host genes and genes acquired from bacterial HGTs to fill gaps in pathways formed by endosymbiont gene loss (Husnik et al., 2013; Luan et al., 2015; Nakabachi et al., 2014; Nikoh and Nakabachi, 2009; Sloan et al., 2014). However, none of these putatively mosaic host-symbiont pathways have been functionally verified.

One of the most complex of these insect-endosymbiont relationships is found in *Planococcus citri*, an insect in a group commonly referred to as mealybugs. The *P. citri* symbiosis exists in an unusual structure (Figure 1A), where a gammaproteobacterium (*Candidatus* Moranella endobia; hereafter *Moranella*) resides in the cytoplasm of a betaproteobacterium (*Candidatus* Tremblaya princeps; hereafter *Tremblaya*), which together exist in specialized insect cells called bacteriocytes (von Dohlen et al., 2001). The *Tremblaya* genome is extremely small and maintains only ~120 protein coding genes, whereas the *Moranella* genome is comparably larger but still encodes only ~400 protein coding genes (López-Madrigal et al., 2013; McCutcheon and von Dohlen, 2011). Complementary patterns of gene loss and retention on the *Tremblaya* and *Moranella* genomes suggest that these two endosymbionts work together to make the essential nutrients required by their host insect (McCutcheon and von Dohlen, 2011). Some of the genes missing on the endosymbiont genomes are found on the insect nuclear genome, the result of numerous HGTs from various bacteria unrelated to either *Tremblaya* or *Moranella* (Husnik et al., 2013).

One potential mosaic biochemical pathway in *P. citri* is that for peptidoglycan (PG) biosynthesis. A PG layer is an almost universal feature of bacteria and is critical for bacterial cell division, shape, and integrity (Errington, 2013; Otten et al., 2018; Typas et al., 2011). Because PG is not produced by eukaryotes but is a nearly ubiquitous feature of bacteria, it is a potent activator of the eukaryotic innate immune response, and the highly conserved PG biosynthetic pathway is the target of many antibiotics (Dziarski, 2003; Otten et al., 2018; Wolf and Underhill, 2018). The presence of numerous HGTs involved in PG synthesis on the nuclear genome of an insect was therefore surprising. Here we test whether mealybugs can use these PG-related

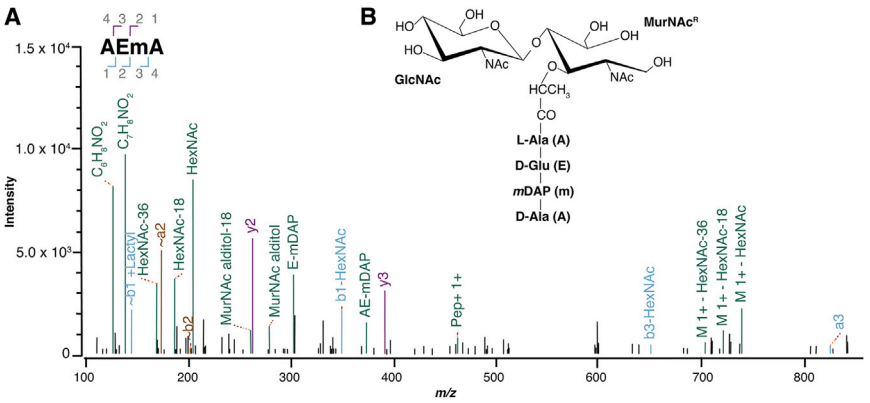

Figure 2. PG Constituent Parts Are Present in Whole Insect Preparations

(A) MS/MS spectrum showing fragments of the tetrapeptide disaccharide shown in (B) as annotated by Byonic (Bern et al., 2017). The label HexNAc indicates that GlcNAc cannot be formally distinguished from the stereochemically identical molecule *N*-acetyl-galactosamine. Pep+ 1+ represents the bare tetrapeptide L-Ala-D-Glu-*m*Dap-D-Ala fragmented from PG glycans, and $C_6H_8NO_2$ and $C_7H_8NO_2$ represent rearrangements of HexNAc after neutral losses such as H_2O.

(B) Schematic of the reduced β-1-4 linked GlcNAc-MurNAc^R disaccharide attached to a tetrapeptide stem made of L-Ala, D-Glu, *m*DAP, and D-Ala.

genes of diverse taxonomic origins and scattered genomic locations to produce a spatially and chemically coherent PG layer.

RESULTS

A Complete PG Pathway Is Predicted by Genomics

The synthesis of a complete PG layer in Gram-negative bacteria can be divided into three classes of reactions based on enzyme location (Figure 1B). The first set of reactions involves the cytoplasmic synthesis of the PG precursor, a β-1,4-linked *N*-acetylglucosamine (GlcNAc)-*N*-acetylmuramic acid (MurNAc) disaccharide linked to an L-alanine (L-Ala)-D-glutamic acid (D-Glu)-*meso*-diaminopimelic acid (*m*Dap)-D-alanine (D-Ala)-D-Ala pentapeptide. The second set of reactions involves inner membrane-associated enzymes that flip this PG precursor into the bacterial periplasm, and the third set of reactions involves the cross-linking of precursor molecules into the growing PG matrix, as well as PG modifications such as trimming the pentapeptide to an L-Ala-D-Glu-*m*Dap-D-Ala tetrapeptide. Our original annotation of the PG biosynthetic pathway of *P. citri* focused on the first two sets of reactions because the *Moranella* genome encoded some of the enzymes required to flip PG into its periplasm, and because the bacterial-to-insect HGTs mostly involved the first set of reactions (Husnik et al., 2013). But our first annotation was not complete; there were unresolved holes in the cytoplasmic part of the pathway, and we paid little attention to the third part of PG synthesis.

In an effort to better understand the functional potential of this mosaic PG biosynthetic pathway, we performed a detailed reannotation of the PG-related genes in this system (Figure 1B; Table S1). Our expanded annotation indicates that a PG layer, if produced, should be comprised of the canonical crosslinked β-1,4-linked GlcNAc-MurNAc disaccharide with an L-Ala-D-Glu-*m*Dap-D-Ala tetrapeptide (Figure 1B; Table S1). Because no genes related to PG biosynthesis are found in the *Tremblaya* genome, we predict that *Tremblaya* should not possess a PG layer.

PG Constituent Parts Are Present in Whole Insect Preparations

We used liquid chromatography coupled to tandem mass spectrometry (LC-MS/MS; Bern et al., 2017) to detect the presence of PG in samples prepared from ~1,500 pooled *P. citri* mealybugs. Ions matching the expected *m/z* values for GlcNAc and MurNAc monomers and dimers, some bound to a tetrapeptide chain (L-Ala-D-Glu-*m*Dap-D-Ala), were identified in the first stage of MS, and the structure of these molecules was confirmed by tandem MS (Figure 2). To rule out the presence of contaminating bacteria in mealybugs as a significant source of PG signal, we performed five replicate 16S rRNA gene amplicon sequencing runs on age-matched insects collected from the same mealybug colony used for LC-MS/MS and a sixth sample taken from a lysate used for MS analysis. On average ~0.61% (range of 0.0604%–4.29%) of all amplicon reads were from bacteria other than *Tremblaya* (76.1% of all reads) and *Moranella* (19.7% of all reads) (Table S2). These results suggest that bacterial contamination is an unlikely source of significant PG signal in our LC-MS/MS experiments. Although these data allow us to conclude that PG is present in the *P. citri-Tremblaya-Moranella* symbiosis, they provide no information on the spatial localization of this putative PG layer.

The PG-Specific Molecule D-Ala Is Specifically Localized at the *Moranella* Periphery

We next attempted to visualize incorporation of D-Ala, a PG-specific molecule, in this symbiosis. Inspired by recent work using localization of fluorescently labeled D-Ala as a proxy for PG biosynthesis (Kuru et al., 2012; Liechti et al., 2014; van Teeseling et al., 2015), we developed a similar approach based on nanometer-scale resolution secondary ion mass spectrometry (nanoSIMS) (Dekas et al., 2016; Dekas and Orphan, 2011). We soaked and injected an ^{15}N-labeled D-Ala solution onto sprouting potatoes on which the mealybugs fed (Figure S1, related to Figure 3). After a week of feeding on labeled potatoes, mealybugs were sacrificed, and the bacteriome tissue was removed and thin-sectioned onto microscope slides. The location of insect bacteriocytes, *Tremblaya*, and *Moranella* cells was first established using fluorescence *in situ* hybridization (FISH) microscopy (Figures 3A and 3F). These FISH-imaged tissue sections were then subjected to nanoSIMS, where we observed strong, specific rings of enriched ^{15}N signal exclusively at or near the periphery of all *Moranella* cells (Figures 3B and 3C–3E). In contrast, mealybugs grown on ^{15}N-labeled L-Ala showed uniform label incorporation throughout the bacteriome tissue, as expected

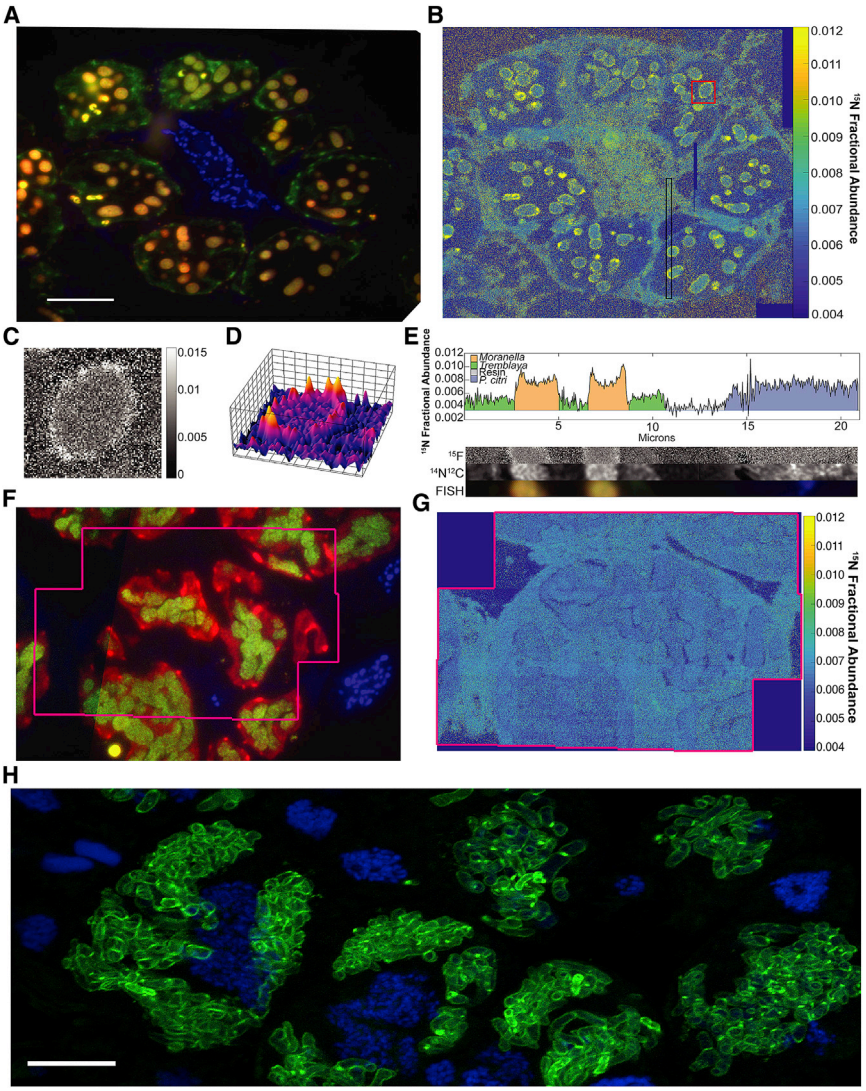

Figure 3. The PG-Specific Molecule D-Ala Is Specifically Localized at the *Moranella* Periphery

(A) FISH imaging of a sectioned bacteriome from a mealybug treated with ^{15}N D-Ala. *Tremblaya* cells are green, *Moranella* cells are yellow-red, and the insect nucleus is blue. Scale bar, 10 μm.

(B) Reconstructed montage of a bacteriocyte from multiple nanoSIMS images shown as a heatmap of the fractional abundance of ^{15}N over ^{14}N [^{15}N/(^{15}N + ^{14}N)] from the same mealybug section depicted in (A); ^{15}N enrichment is observed as yellow rings around the edges of *Moranella* cells.

(C) Close-up of a single *Moranella* cell highlighted in the red box in (B) shows enrichment of ^{15}N D-Ala along *Moranella's* periphery.

(D) Three-dimensional representation of ^{15}N D-Ala enrichment of the *Moranella* cell shown in (C).

(E) A cross section through a portion of the bacteriocyte (black rectangle in B) reveals less ^{15}N enrichment in either *Tremblaya* (green) or the insect tissue (blue) as compared with *Moranella* (orange). The row labeled ^{15}F is the fractional abundance of ^{15}N over ^{14}N [^{15}N/(^{15}N + ^{14}N)], the ^{14}N/^{12}C row depicts the ratio of the abundant natural isotope ^{14}N over the common isotope ^{12}C, and the bottom row shows this section of tissue in FISH microscopy.

(F) FISH imaging of a sectioned bacteriome from a control mealybug treated with ^{15}N L-Ala. *Tremblaya* cells are red, *Moranella* cells are green, and insect nuclei are blue.

(G) The fractional abundance of ^{15}N L-Ala as detected by nanoSIMS from the portion of (F) outlined in the pink box. The signal of ^{15}N L-Ala is nearly uniform throughout the three organisms represented in this tissue, as expected for a molecule that is uniformly incorporated into protein.

(H) Representative confocal image of Cu-catalyzed click-chemistry to a D-Ala variant showing enrichment at the *Moranella* periphery (green). Insect nuclei are stained with DAPI (blue). Image is comprised of four merged slices from a z stack. Scale bar, 10 μm.

because L-Ala should be incorporated without bias into all proteins in the symbiosis (Figures 3F and 3G). We verified a *Moranella* periphery-specific pattern of D-Ala enrichment using bioorthogonal, Cu-catalyzed click-chemistry and fluorescence microscopy (Figure 3H; Kuru et al., 2012; Liechti et al., 2014; van Teeseling et al., 2015). The localization of enriched D-Ala signal at the cell periphery of *Moranella*, but not *Tremblaya* or the insect tissue, in both nanoSIMS and fluorescent microscopy is consistent with our genomic prediction that PG production should be specifically localized to the *Moranella* periphery, but should not exist in *Tremblaya* (Figure 1B). Similar patterns of D-Ala enrichment are routinely interpreted as strong evidence for PG biosynthesis in bacteria (Kuru et al., 2012; Liechti et al., 2014; van Teeseling et al., 2015).

A PG-Targeting Antibiotic Specifically Affects the *Moranella* Cell Envelope

Our nanoSIMS and click fluorescence data show that the *P. citri* PG layer is specifically located at the *Moranella* periphery, but both nanoSIMS and light microscopy lack the spatial resolution to place this PG signal precisely in the periplasm of *Moranella*. To provide additional evidence that the PG layer we observe is located in the periplasm of *Moranella*, we fed age-matched mealybugs on diets with and without the antibiotic cefsulodin, which specifically targets the periplasmic-localized penicillin-binding protein, Pbp1B. The gene for Pbp1B is encoded on the *Moranella* genome (Figure 1B; Table S1). Pbp1B functions as a glycosyltransferase and transpeptidase, joining new GlcNAc-MurNAc-pentapeptide precursors to the nascent PG matrix in the periplasm (Cho et al., 2014; Typas et al., 2011). A common phenotype for bacterial cells grown in hypotonic media in the presence of antibiotics is membrane blebbing and cell lysis, although the exact responses vary considerably in different bacteria (Chung et al., 2009; Yao et al., 2012). Given that *Moranella* lives exclusively in the cytoplasm of another bacterium, and therefore likely in an isotonic environment, we suspected that any antibiotic-related phenotype we might observe would be subtle. Using

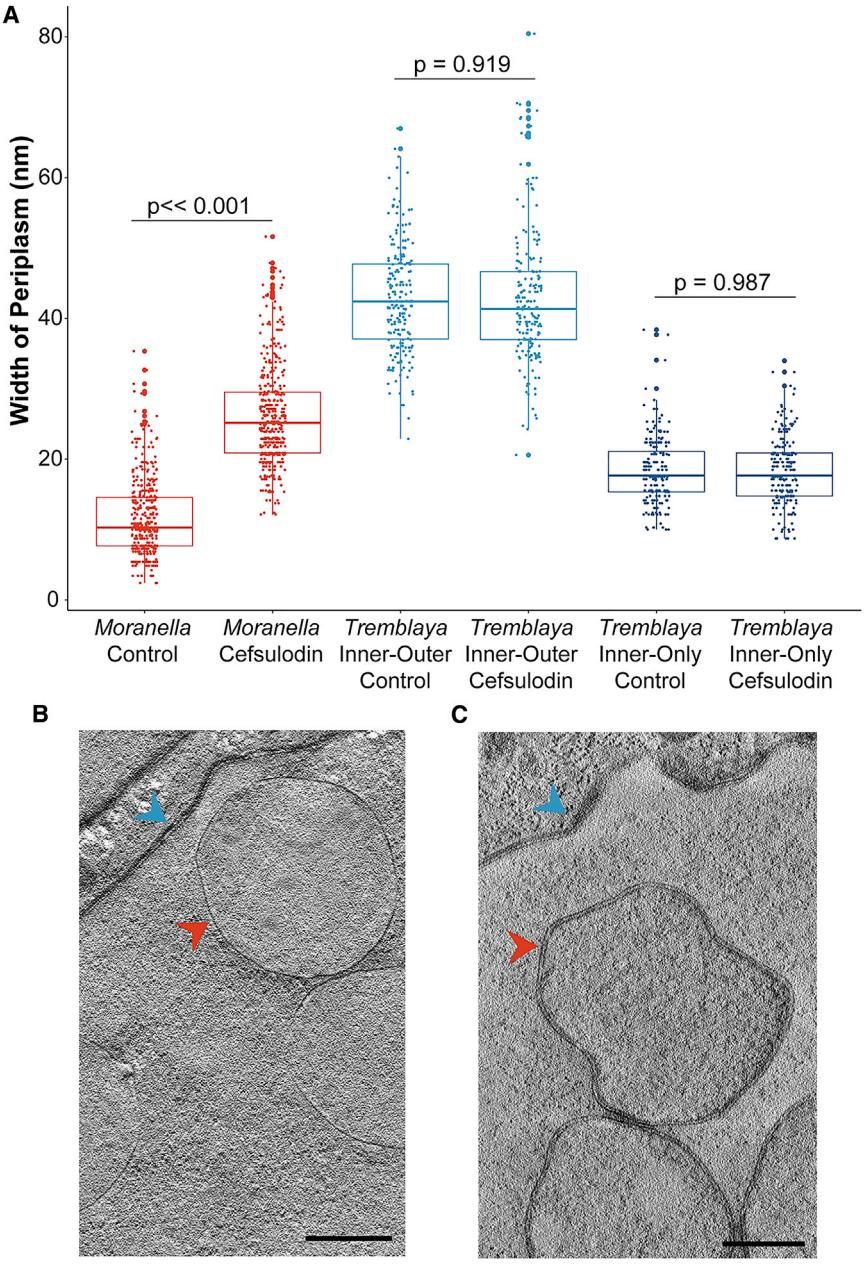

Figure 4. A PG-Targeting Antibiotic Specifically Affects the *Moranella* Cell Envelope

(A) Quantification of the distance between the inner- and outer-most membranes of *Tremblaya* (n = 200) and *Moranella* (n = 400) and the inner two membranes of *Tremblaya* (n = 200) from control and cefsulodin-treated insects; mean ± SEM with a jitter plot of all data points. All data points were collected from random sections from two independent biological replicates. There is a significant difference only in the periplasmic space of *Moranella*, 11.5 versus 26.1 nm (Student's t test) with an effect size of 2.3. The effect sizes for *Tremblaya*'s inner-only and inner-to-outer measurements were 0.0016 and 0.034, respectively.

(B and C) Representative TEM images of control (B) and 100 μg/mL cefsulodin-treated (C) insects with *Tremblaya* (blue arrow) and *Moranella* (red arrow) membranes visible.

See also Table S3.

transmission electron microscopy (TEM), we found that the periplasmic space of *Moranella* was specifically enlarged in the presence of cefsulodin versus control animals (Figures 4A and 4C). Because *Tremblaya* has three membranes, we also measured both the distance between the inner two and from the innermost to the outermost membranes as a control. No significant changes in membrane spacing were observed in *Tremblaya* between control and cefsulodin treatment (Figures 4A and 4B), indicating that this membrane spacing phenotype is specific to *Moranella* and not simply due to a general disruption of mealybug health in the presence of antibiotics.

A PG-Related HGT of Alphaproteobacterial Origin Is Localized to the *Moranella* Cytoplasm

Because most of the genes involved in the cytoplasmic portion of PG synthesis exist as HGTs on the insect genome (Figure 1B), it is formally possible that the GlcNAc-MurNAc-pentapeptide PG precursor is produced in the insect cytoplasm and then transported into *Moranella*. We suspected, however, that it was more likely that these HGTs were first translated in the insect tissue and then transported as proteins into the *Moranella* cytoplasm to produce the PG precursor molecule. This suspicion is primarily based on previous results from another related insect, where the protein product of an HGT on the pea aphid genome was shown to be transported into the cytoplasm of its bacterial endosymbiont, *Buchnera aphidicola* (Nakabachi et al., 2014). We note that if the PG layer we report here is located in the *Moranella* periplasm, and if it is constructed in the *Moranella* cytoplasm as we predict in Figure 1B, the proteins that result from HGT to the insect genome and that function in the *Moranella* cytoplasm must cross five lipid bilayers to get there: *Tremblaya* has three lipid bilayers, and *Moranella* has two (von Dohlen et al., 2001) (Figure 1A).

In order to differentiate between these two scenarios for PG precursor production, we produced a polyclonal antibody to a predicted protein encoded by a bacteria-to-insect HGT and observed its localization to test whether it was found in the *Moranella* cytoplasm. The antibody was generated against a peptide fragment of MurF, a ligase that normally functions in the bacterial cytoplasm to join D-Ala-D-Ala to the MurNAc-linked

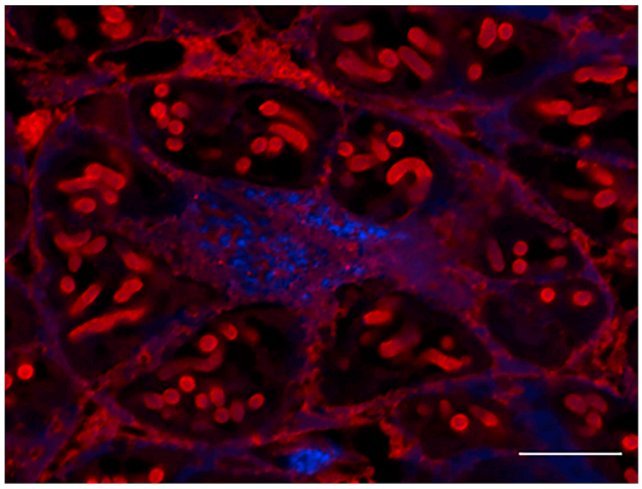

Figure 5. MurF, a PG-Related HGT of Alphaproteobacterial Origin, Is Localized to the *Moranella* Cytoplasm

Representative confocal image of a sectioned bacteriome stained with an anti-MurF antibody (red). Insect nuclei are stained with Hoechst (blue). Signal is detected inside of the *Moranella* cells and insect tissue, but not *Tremblaya*. Scale bar, 10 μm.

tripeptide to produce the pentapeptide (Otten et al., 2018; Typas et al., 2011). In the *P. citri* symbiosis, the *murF* gene exists only as an HGT that was transferred from an alphaproteobacterium to the host insect nuclear genome (Figure 1B; Husnik et al., 2013). Immunohistochemistry on paraffin-embedded insect tissue showed that MurF is found uniformly throughout the cytoplasm of *Moranella* and in portions of the insect tissue, but is completely missing from the *Tremblaya* cytoplasm (Figure 5). The restriction of signal to the insect and *Moranella* cytoplasm is consistent with the hypothesis that the insect makes MurF and transports it into *Moranella* as a protein but does not appreciably accumulate in *Tremblaya*. This localization pattern suggests that genes resulting from HGTs on the *P. citri* nuclear genome can be made into proteins by host machinery and can be transported across the three lipid bilayers of *Tremblaya* and the two lipid bilayers of *Moranella* to end up in the *Moranella* cytoplasm. We note it is formally possible that the *murF* mRNA, not protein, is transported into *Moranella* and then translated by *Moranella* ribosomes. The data in Figure 5 also suggest that PG is made entirely in *Moranella* and that the alternative scenario, where PG precursors are built in the insect cytoplasm and transported into *Moranella*, is unlikely.

Collectively, our data from LC-MS/MS experiments (Figure 2), nanoSIMS (Figures 3B–3E and 3G), fluorescence microscopy (Figure 3H), antibiotic treatments (Figure 4), and immunohistochemistry (Figure 5) allow us to conclude that the genetic mosaic depicted in Figure 1B is functional and produces a PG layer that is likely built in the *Moranella* cytoplasm and located in the *Moranella* periplasm.

DISCUSSION

A PG-based cell wall is an ancient and defining feature of bacteria. Not surprisingly, the highly conserved set of genes that encode PG biosynthesis is normally exclusively found on bacterial genomes. Until now, there were two known exceptions to this pattern, both related to cyanobacterial-derived endosymbionts of photosynthetic eukaryotes. The first example of PG-related HGT comes from the "chromatophore" of the rhizarian protist *Paulinella chromatophora*. EM suggests that the *Paulinella* chromatophore has a PG layer (Kies, 1974), which is encoded primarily on the chromatophore genome with the exception of one bacterial HGT to the host protist genome (Nowack et al., 2016). The second example comes from the group of photosynthetic eukaryotes whose ancestor formed the original endosymbiosis with the cyanobacterium that became the chloroplast. This group, called the Archaeplastida, includes land plants, red algae, green algae, and glaucophyte algae (Lane and Archibald, 2008; McFadden, 2001). Many archaeplastidal nuclear genomes encode some PG-related EGT and HGTs (van Baren et al., 2016; Sato and Takano, 2017), but these genes do not always seem to work together to form a functional PG layer at the chloroplast periphery. A chloroplast-localized PG layer has been verified using fluorescently labeled D-Ala in the moss *Physcomitrella patens* (Hirano et al., 2016), and possible chloroplast PG layers have been observed by EM in glaucophytes (Schenk, 1970). But in the land plant *Arabidopsis thaliana*, which retains some PG-related genes on its nuclear genome, although fewer than in the moss *P. patens*, no PG layer exists at the chloroplast periphery and at least one PG-related enzyme has been coopted for a different function (Garcia et al., 2008). These results serve as a cautionary note about inferring function from the presence of HGTs alone: gene presence is not a reliable predictor of biological function (Doolittle, 2013).

Exactly how the *Moranella* PG layer is built, its function, and its precise cellular location remain unknown. One important remaining question is the source of D-Ala and D-Glu in *Moranella*'s PG. Our original annotation left the activities of Alr (alanine racemase) and MurI (glutamate racemase) unaccounted for: they did not exist as HGTs on the insect genome, and they were not present on the *Moranella* genome (Husnik et al., 2013). Our new annotation confirms that homologs of these genes are missing in the *P. citri* symbiosis. Interestingly, GlyA and MetC have been shown to moonlight as alanine racemases in *Chlamydia trachomatis* and *Escherichia coli*, respectively (De Benedetti et al., 2014; Kang et al., 2011; Otten et al., 2018), and we find eukaryotic homologs for these genes on the mealybug genome (Table S1). Similarly, DapF has been shown to moonlight as a glutamate racemase in *C. trachomatis* (Liechti et al., 2018), and this gene exists as an HGT of alphaproteobacterial origin on the *P. citri* genome (Husnik et al., 2013). These data suggest that the loss of *alr* in *Moranella* may be compensated by a moonlighting insect enzyme, and that the loss of *dapF* on the *Moranella* genome may be compensated for by a moonlighting alphaproteobacterial *dapF* HGT (Table S1). But it is also possible that the source of D-Ala and D-Glu is not from these putatively moonlighting enzymes at all, but rather from either the plant sap diet of the insect or from D-amino acids in *P. citri* produced from normal insect biochemistry. Although not studied extensively, D-amino acids have been found in both plants (Robinson, 1976) and insects (Auclair and Patton, 1950; Corrigan and Srinivasan, 1966; Corrigan,

1969), although to our knowledge the levels of these compounds have not been measured in *P. citri*. The source(s) of D-Ala and D-Glu in *Moranella* could therefore be from the diet of the insect, the insect's native amino acid biochemistry, moonlighting enzymes of various origins, or from some combination of all of these sources.

Our MurF immunohistochemistry localization data show that the protein products of HGTs on the insect genome can be specifically targeted to the *Moranella* cytoplasm (Figure 5). Import of enzymes (or mRNA) to the *Moranella* cytoplasm for precursor production rather than producing the GlcNAc-MurNAc-pentapeptide precursor in the insect cytoplasm may limit the risk to the insect host of triggering a PG-based immune response. Other insects with long-term endosymbionts devote resources to scavenging PG fragments in order to prevent continuous immune activation (Maire et al., 2019). By apparently sequestering PG production to inside of *Moranella*, *P. citri* may avoid the need for such contingency pathways, at least until *Moranella* cells are recycled near the end of the mealybug's life (Kono et al., 2008).

It is notable that most of the proteins made from PG-related HGTs on the insect genome are predicted to function in the cytoplasmic part of PG synthesis, whereas the PG-related genes retained by *Moranella* all code for inner membrane- or periplasm-associated proteins (Figure 1B). These patterns of gene loss, gene retention, and HGT suggest that genes encoding proteins that function in the *Moranella* cytoplasm are more likely to be successfully transferred to the host insect nucleus. It is tempting to speculate that these HGT and protein localization patterns reflect the (currently unknown) mechanism used by the symbiosis to traffic proteins or RNAs made from the host genome to the correct subcellular compartment. It may be that this trafficking mechanism can transport soluble proteins and RNA, but is unable to transfer membrane-associated proteins. Whatever the trafficking mechanism, our data show that these proteins of foreign genomic origin, now encoded on the insect genome, work together with proteins still encoded on the *Moranella* genome to produce a genuine PG layer at the *Moranella* periphery. Future work will be required to definitively locate the *Moranella* PG layer because our current experiments lack the resolution to place this PG layer precisely in the *Moranella* periplasm.

Although the exact role that this PG layer plays in the *P. citri* symbiosis remains unknown, work from plastids suggests that host takeover of endosymbiont PG production can be an important step in the regulation of endosymbiont cell division and potentially further integration with the host organism (de Vries and Gould, 2018). In moss, knocking out a PG-related HGT on the nuclear genome results in enlarged chloroplasts (Machida et al., 2006), and treatment with various PG-targeting antibiotics results in fewer and larger chloroplasts per host cell (Katayama et al., 2003). Together these data suggest that the movement of PG-related genes from organelle genome to the host is a way for hosts to regulate organelle division (de Vries and Gould, 2018; Katayama et al., 2003; Machida et al., 2006). In *P. citri* mealybugs, *Tremblaya* was acquired before *Moranella* (Hardy et al., 2008; Thao et al., 2002), and so the host insect must have found a way of controlling *Tremblaya* as the sole endosymbiont prior to the acquisition of *Moranella*. Because the patterns of HGT and protein targeting we observe here are strongly convergent with moss chloroplasts (Garcia et al., 2008; Katayama et al., 2003; Machida et al., 2006), it is tempting to speculate that the function is also convergent; that is, PG-related HGTs have been retained on the insect genome as a way of controlling the cell division of a bacterium that lives inside of another bacterium inside of insect cells.

The frequency and importance of bacteria-to-eukaryote HGT are a matter of debate (Husnik and McCutcheon, 2018; Martin, 2017; Martin and Herrmann, 1998). Although in our view numerous studies using genomic and transcriptomic data strongly support the idea that bacteria-to-eukaryote HGT is common in some groups of eukaryotes and is likely to be biologically significant (Husnik and McCutcheon, 2018), functional validation of most of these HGTs is lacking. In some cases, HGTs involving single-step (or single operon) biochemical functions have been experimentally validated by *in vitro* protein expression, enzymatic assays, and/or *in situ* RNAi (Chou et al., 2015; Dean et al., 2018; Kominek et al., 2019; Metcalf et al., 2014; Milner et al., 2019; Moran and Jarvik, 2010; Stairs et al., 2018). Although these examples serve as important milestones in HGT research, none approaches the genetic complexity we describe here, which is more akin to the host-organelle genetic mosaic used by eukaryotes to build proto-heme (Kořený et al., 2013; Oborník and Green, 2005). Our data show that multigene, multi-genome, and multi-cellular compartment conglomerations are not unique to organelles (Booth and Doolittle, 2015a; McCutcheon and Keeling, 2014; but see Lane and Martin, 2015 and Booth and Doolittle, 2015b), and that cell biological, genetic, and biochemical mosaics can become functional in examples outside of the mitochondrion and plastid.

STAR★METHODS

Detailed methods are provided in the online version of this paper and include the following:

- KEY RESOURCES TABLE
- LEAD CONTACT AND MATERIALS AVAILABILITY
- EXPERIMENTAL MODEL AND SUBJECT DETAILS
  - Mealybugs
- METHOD DETAILS
  - Gene annotation
  - Mealybug feeding and dissection
  - LC-MS/MS
  - 16S rRNA sequencing
  - FISH-nanoSIMS
  - Cu-click chemistry
  - TEM and dual-axis tomography
  - Immunohistochemistry
- QUANTIFICATION AND STATISTICAL ANALYSIS
  - Membrane measurements
- DATA AND CODE AVAILABILITY

SUPPLEMENTAL INFORMATION

Supplemental Information can be found online at https://doi.org/10.1016/j.cell.2019.08.054.

ACKNOWLEDGMENTS

We thank Bil Clemons for helpful discussions about PG; Denghui David Xing of the University of Montana Genomics Core for sequencing expertise; Carol Garland, Matthew Hunt, and the Caltech Kavli Nanoscience Institute for aid in maintaining the TF-30 electron microscope; and the Gordon and Betty Moore and Beckman Foundations for gifts to Caltech to support electron microscopy. PG Mass spectrometry analyses were performed by the biOMICS Facility of the Faculty of Science Mass Spectrometry Centre at the University of Sheffield. We thank Adelina E. Acosta-Martin and Ankur Patel for their help with peptidoglycan analyses. This work was supported by the Gordon and Betty Moore Foundation (GBMF5602), the National Aeronautics and Space Administration Astrobiology Institute (NNA15BB04A), the National Science Foundation (IOS-1553529), and the Biotechnology and Biological Sciences Research Council (BB/N000951/1 and 2058718).

AUTHOR CONTRIBUTIONS

D.C.B.: conceptualization, investigation, analysis, methodology, validation, visualization, and writing; G.L.C. and J.S.M.: investigation, methodology, analysis, validation, visualization, and writing; K.M.S.: conceptualization, analysis, methodology, investigation, resources, and writing; S.M.: analysis, methodology, resources, software, and writing; D.M.B.: investigation, methodology, and visualization; M.S.L.: investigation, methodology, resources, validation, and visualization; A.I.G.: data curation, analysis, investigation, software, and visualization; P.J.B.: methodology, resources, and administration; V.J.O.: conceptualization, funding acquisition, resources, and administration; J.P.M.: conceptualization, funding acquisition, administration, resources, visualization, and writing.

DECLARATION OF INTERESTS

The authors declare no competing interests.

Received: June 18, 2019
Revised: August 6, 2019
Accepted: August 28, 2019
Published: October 3, 2019

REFERENCES

Akman Gündüz, E., and Douglas, A.E. (2009). Symbiotic bacteria enable insect to use a nutritionally inadequate diet. Proc. Biol. Sci. *276*, 987–991.

Altschul, S.F., Gish, W., Miller, W., Myers, E.W., and Lipman, D.J. (1990). Basic local alignment search tool. J. Mol. Biol. *215*, 403–410.

Auclair, J.L., and Patton, R.L. (1950). On the occurrence of d-Alanine in the haemolymph of the milkweed bug, *oncopeltus fasciatus*. Rev. Can. Biol. *9*, 3–8.

Baumann, P. (2005). Biology bacteriocyte-associated endosymbionts of plant sap-sucking insects. Annu. Rev. Microbiol. *59*, 155–189.

Bern, M., Beniston, R., and Mesnage, S. (2017). Towards an automated analysis of bacterial peptidoglycan structure. Anal. Bioanal. Chem. *409*, 551–560.

Bolger, A.M., Lohse, M., and Usadel, B. (2014). Trimmomatic: a flexible trimmer for Illumina sequence data. Bioinformatics *30*, 2114–2120.

Booth, A., and Doolittle, W.F. (2015a). Eukaryogenesis, how special really? Proc. Natl. Acad. Sci. USA *112*, 10278–10285.

Booth, A., and Doolittle, W.F. (2015b). Reply to Lane and Martin: Being and becoming eukaryotes. Proc. Natl. Acad. Sci. USA *112*, E4824.

Cho, H., Uehara, T., and Bernhardt, T.G. (2014). Beta-lactam antibiotics induce a lethal malfunctioning of the bacterial cell wall synthesis machinery. Cell *159*, 1300–1311.

Chou, S., Daugherty, M.D., Peterson, S.B., Biboy, J., Yang, Y., Jutras, B.L., Fritz-Laylin, L.K., Ferrin, M.A., Harding, B.N., Jacobs-Wagner, C., et al. (2015). Transferred interbacterial antagonism genes augment eukaryotic innate immune function. Nature *518*, 98–101.

Chung, H.S., Yao, Z., Goehring, N.W., Kishony, R., Beckwith, J., and Kahne, D. (2009). Rapid β-lactam-induced lysis requires successful assembly of the cell division machinery. Proc. Natl. Acad. Sci. USA *106*, 21872–21877.

Cimino, M., Alamo, L., and Salazar, L. (2006). Permeabilization of the mycobacterial envelope for protein cytolocalization studies by immunofluorescence microscopy. BMC Microbiol. *6*, 35.

Corrigan, J.J. (1969). D-amino acids in animals. Science *164*, 142–149.

Corrigan, J.J., and Srinivasan, N.G. (1966). The occurrence of certain D-amino acids in insects. Biochemistry *5*, 1185–1190.

De Benedetti, S., Bühl, H., Gaballah, A., Klöckner, A., Otten, C., Schneider, T., Sahl, H.-G., and Henrichfreise, B. (2014). Characterization of serine hydroxymethyltransferase GlyA as a potential source of D-alanine in *Chlamydia pneumoniae*. Front. Cell. Infect. Microbiol. *4*, 19.

de Vries, J., and Gould, S.B. (2018). The monoplastidic bottleneck in algae and plant evolution. J. Cell Sci. *131*, jcs203414.

Dean, P., Sendra, K.M., Williams, T.A., Watson, A.K., Major, P., Nakjang, S., Kozhevnikova, E., Goldberg, A.V., Kunji, E.R.S., Hirt, R.P., and Embley, T.M. (2018). Transporter gene acquisition and innovation in the evolution of Microsporidia intracellular parasites. Nat. Commun. *9*, 1709.

Dekas, A.E., and Orphan, V.J. (2011). Identification of diazotrophic microorganisms in marine sediment via fluorescence *in situ* hybridization coupled to nanoscale secondary ion mass spectrometry (FISH-NanoSIMS). Methods Enzymol. *486*, 281–305.

Dekas, A.E., Connon, S.A., Chadwick, G.L., Trembath-Reichert, E., and Orphan, V.J. (2016). Activity and interactions of methane seep microorganisms assessed by parallel transcription and FISH-NanoSIMS analyses. ISME J. *10*, 678–692.

Doolittle, W.F. (2013). Is junk DNA bunk? A critique of ENCODE. Proc. Natl. Acad. Sci. USA *110*, 5294–5300.

Duchêne, A.-M., Giritch, A., Hoffmann, B., Cognat, V., Lancelin, D., Peeters, N.M., Zaepfel, M., Maréchal-Drouard, L., and Small, I.D. (2005). Dual targeting is the rule for organellar aminoacyl-tRNA synthetases in *Arabidopsis thaliana*. Proc. Natl. Acad. Sci. USA *102*, 16484–16489.

Dunning Hotopp, J.C. (2011). Horizontal gene transfer between bacteria and animals. Trends Genet. *27*, 157–163.

Dunning Hotopp, J.C., and Estes, A.M. (2014). Biology wars: the eukaryotes strike back. Cell Host Microbe *16*, 701–703.

Dziarski, R. (2003). Recognition of bacterial peptidoglycan by the innate immune system. Cell. Mol. Life Sci. *60*, 1793–1804.

Errington, J. (2013). L-form bacteria, cell walls and the origins of life. Open Biol. *3*, 120143.

Fuchs, B.M., Pernthaler, J., and Amann, R. (2007). Cell identification by fluorescence in situ hybridization. In Methods for General and Molecular Microbiology, Third Edition, C.A. Reddy, T.J. Beveridge, J.A. Breznak, G.A. Marzluf, T.M. Schmidt, and L.R. Snyder, eds. (ASM Press), pp. 886–896.

Gabaldón, T. (2018). Relative timing of mitochondrial endosymbiosis and the "pre-mitochondrial symbioses" hypothesis. IUBMB Life *70*, 1188–1196.

Garcia, M., Myouga, F., Takechi, K., Sato, H., Nabeshima, K., Nagata, N., Takio, S., Shinozaki, K., and Takano, H. (2008). An Arabidopsis homolog of the bacterial peptidoglycan synthesis enzyme MurE has an essential role in chloroplast development. Plant J. *53*, 924–934.

Gray, M.W. (2015). Mosaic nature of the mitochondrial proteome: Implications for the origin and evolution of mitochondria. Proc. Natl. Acad. Sci. USA *112*, 10133–10138.

Hardy, N.B., Gullan, P.J., and Hodgson, C.J. (2008). A subfamily-level classification of mealybugs (Hemiptera: Pseudococcidae) based on integrated molecular and morphological data. Syst. Entomol. *33*, 51–71.

Hirano, T., Tanidokoro, K., Shimizu, Y., Kawarabayasi, Y., Ohshima, T., Sato, M., Tadano, S., Ishikawa, H., Takio, S., Takechi, K., and Takano, H. (2016). Moss chloroplasts are surrounded by a peptidoglycan wall containing D-amino acids. Plant Cell *28*, 1521–1532.

Holben, W.E., Williams, P., Gilbert, M., Saarinen, M., Särkilahti, L.K., and Apajalahti, J.H. (2002). Phylogenetic analysis of intestinal microflora indicates a novel Mycoplasma phylotype in farmed and wild salmon. Microb. Ecol. *44*, 175–185.

Husnik, F., and McCutcheon, J.P. (2018). Functional horizontal gene transfer from bacteria to eukaryotes. Nat. Rev. Microbiol. *16*, 67–79.

Husnik, F., Nikoh, N., Koga, R., Ross, L., Duncan, R.P., Fujie, M., Tanaka, M., Satoh, N., Bachtrog, D., Wilson, A.C.C., et al. (2013). Horizontal gene transfer from diverse bacteria to an insect genome enables a tripartite nested mealybug symbiosis. Cell *153*, 1567–1578.

Kang, L., Shaw, A.C., Xu, D., Xia, W., Zhang, J., Deng, J., Wöldike, H.F., Liu, Y., and Su, J. (2011). Upregulation of MetC is essential for D-alanine-independent growth of an alr/dadX-deficient *Escherichia coli* strain. J. Bacteriol. *193*, 1098–1106.

Katayama, N., Takano, H., Sugiyama, M., Takio, S., Sakai, A., Tanaka, K., Kuroiwa, H., and Ono, K. (2003). Effects of antibiotics that inhibit the bacterial peptidoglycan synthesis pathway on moss chloroplast division. Plant Cell Physiol. *44*, 776–781.

Keeling, P.J., and Palmer, J.D. (2008). Horizontal gene transfer in eukaryotic evolution. Nat. Rev. Genet. *9*, 605–618.

Kies, L. (1974). [Electron microscopical investigations on Paulinella chromatophora Lauterborn, a thecamoeba containing blue-green endosymbionts (Cyanelles) (author's transl)]. Protoplasma *80*, 69–89.

Koga, R., Meng, X.-Y., Tsuchida, T., and Fukatsu, T. (2012). Cellular mechanism for selective vertical transmission of an obligate insect symbiont at the bacteriocyte-embryo interface. Proc. Natl. Acad. Sci. USA *109*, E1230–E1237.

Kominek, J., Doering, D.T., Opulente, D.A., Shen, X.-X., Zhou, X., DeVirgilio, J., Hulfachor, A.B., Groenewald, M., Mcgee, M.A., Karlen, S.D., et al. (2019). Eukaryotic acquisition of a bacterial operon. Cell *176*, 1356–1366.e10.

Kono, M., Koga, R., Shimada, M., and Fukatsu, T. (2008). Infection dynamics of coexisting beta- and gammaproteobacteria in the nested endosymbiotic system of mealybugs. Appl. Environ. Microbiol. *74*, 4175–4184.

Koonin, E.V., Makarova, K.S., and Aravind, L. (2001). Horizontal gene transfer in prokaryotes: quantification and classification. Annu. Rev. Microbiol. *55*, 709–742.

Kořený, L., Oborník, M., and Lukeš, J. (2013). Make it, take it, or leave it: heme metabolism of parasites. PLoS Pathog. *9*, e1003088.

Kozich, J.J., Westcott, S.L., Baxter, N.T., Highlander, S.K., and Schloss, P.D. (2013). Development of a dual-index sequencing strategy and curation pipeline for analyzing amplicon sequence data on the MiSeq Illumina sequencing platform. Appl. Environ. Microbiol. *79*, 5112–5120.

Kremer, J.R., Mastronarde, D.N., and McIntosh, J.R. (1996). Computer visualization of three-dimensional image data using IMOD. J. Struct. Biol. *116*, 71–76.

Ku, C., Nelson-Sathi, S., Roettger, M., Sousa, F.L., Lockhart, P.J., Bryant, D., Hazkani-Covo, E., McInerney, J.O., Landan, G., and Martin, W.F. (2015). Endosymbiotic origin and differential loss of eukaryotic genes. Nature *524*, 427–432.

Kuru, E., Hughes, H.V., Brown, P.J., Hall, E., Tekkam, S., Cava, F., de Pedro, M.A., Brun, Y.V., and VanNieuwenhze, M.S. (2012). In Situ probing of newly synthesized peptidoglycan in live bacteria with fluorescent D-amino acids. Angew. Chem. Int. Ed. Engl. *51*, 12519–12523.

Lane, C.E., and Archibald, J.M. (2008). The eukaryotic tree of life: endosymbiosis takes its TOL. Trends Ecol. Evol. *23*, 268–275.

Lane, N., and Martin, W.F. (2015). Eukaryotes really are special, and mitochondria are why. Proc. Natl. Acad. Sci. USA *112*, E4823.

Liechti, G.W., Kuru, E., Hall, E., Kalinda, A., Brun, Y.V., VanNieuwenhze, M., and Maurelli, A.T. (2014). A new metabolic cell-wall labelling method reveals peptidoglycan in *Chlamydia trachomatis*. Nature *506*, 507–510.

Liechti, G., Singh, R., Rossi, P.L., Gray, M.D., Adams, N.E., and Maurelli, A.T. (2018). *Chlamydia trachomatis* dapF encodes a bifunctional enzyme capable of both D-glutamate racemase and diaminopimelate epimerase activities. MBio *9*, e00204–e00218.

López-Madrigal, S., Latorre, A., Porcar, M., Moya, A., and Gil, R. (2013). Mealybugs nested endosymbiosis: going into the 'matryoshka' system in *Planococcus citri* in depth. BMC Microbiol. *13*, 74.

Luan, J.-B., Chen, W., Hasegawa, D.K., Simmons, A.M., Wintermantel, W.M., Ling, K.-S., Fei, Z., Liu, S.-S., and Douglas, A.E. (2015). Metabolic coevolution in the bacterial symbiosis of whiteflies and related plant sap-feeding insects. Genome Biol. Evol. *7*, 2635–2647.

Machida, M., Takechi, K., Sato, H., Chung, S.J., Kuroiwa, H., Takio, S., Seki, M., Shinozaki, K., Fujita, T., Hasebe, M., and Takano, H. (2006). Genes for the peptidoglycan synthesis pathway are essential for chloroplast division in moss. Proc. Natl. Acad. Sci. USA *103*, 6753–6758.

Maire, J., Vincent-Monégat, C., Balmand, S., Vallier, A., Hervé, M., Masson, F., Parisot, N., Vigneron, A., Anselme, C., Perrin, J., et al. (2019). Weevil *pgrp-lb* prevents endosymbiont TCT dissemination and chronic host systemic immune activation. Proc. Natl. Acad. Sci. USA *116*, 5623–5632.

Martin, W.F. (2017). Too much eukaryote LGT. BioEssays *39*, 1700115.

Martin, W., and Herrmann, R.G. (1998). Gene transfer from organelles to the nucleus: how much, what happens, and Why? Plant Physiol. *118*, 9–17.

Martin, W., Rujan, T., Richly, E., Hansen, A., Cornelsen, S., Lins, T., Leister, D., Stoebe, B., Hasegawa, M., and Penny, D. (2002). Evolutionary analysis of *Arabidopsis*, cyanobacterial, and chloroplast genomes reveals plastid phylogeny and thousands of cyanobacterial genes in the nucleus. Proc. Natl. Acad. Sci. USA *99*, 12246–12251.

Mastronarde, D.N. (2005). Automated electron microscope tomography using robust prediction of specimen movements. J. Struct. Biol. *152*, 36–51.

McCutcheon, J.P. (2016). From microbiology to cell biology: when an intracellular bacterium becomes part of its host cell. Curr. Opin. Cell Biol. *41*, 132–136.

McCutcheon, J.P., and Keeling, P.J. (2014). Endosymbiosis: protein targeting further erodes the organelle/symbiont distinction. Curr. Biol. *24*, R654–R655.

McCutcheon, J.P., and Moran, N.A. (2011). Extreme genome reduction in symbiotic bacteria. Nat. Rev. Microbiol. *10*, 13–26.

McCutcheon, J.P., and von Dohlen, C.D. (2011). An interdependent metabolic patchwork in the nested symbiosis of mealybugs. Curr. Biol. *21*, 1366–1372.

McFadden, G.I. (2001). Primary and secondary endosymbiosis and the origin of plastids. J. Phycol. *37*, 951–959.

Metcalf, J.A., Funkhouser-Jones, L.J., Brileya, K., Reysenbach, A.-L., and Bordenstein, S.R. (2014). Antibacterial gene transfer across the tree of life. eLife *3*, e04266.

Milner, D.S., Attah, V., Cook, E., Maguire, F., Savory, F.R., Morrison, M., Müller, C.A., Foster, P.G., Talbot, N.J., Leonard, G., and Richards, T.A. (2019). Environment-dependent fitness gains can be driven by horizontal gene transfer of transporter-encoding genes. Proc. Natl. Acad. Sci. USA *116*, 5613–5622.

Moran, N.A., and Bennett, G.M. (2014). The tiniest tiny genomes. Annu. Rev. Microbiol. *68*, 195–215.

Moran, N.A., and Jarvik, T. (2010). Lateral transfer of genes from fungi underlies carotenoid production in aphids. Science *328*, 624–627.

Moran, N.A., Tran, P., and Gerardo, N.M. (2005). Symbiosis and insect diversification: an ancient symbiont of sap-feeding insects from the bacterial phylum Bacteroidetes. Appl. Environ. Microbiol. *71*, 8802–8810.

Nakabachi, A., Ishida, K., Hongoh, Y., Ohkuma, M., and Miyagishima, S.-Y. (2014). Aphid gene of bacterial origin encodes a protein transported to an obligate endosymbiont. Curr. Biol. *24*, R640–R641.

Neupert, W., and Herrmann, J.M. (2007). Translocation of proteins into mitochondria. Annu. Rev. Biochem. *76*, 723–749.

Nikoh, N., and Nakabachi, A. (2009). Aphids acquired symbiotic genes via lateral gene transfer. BMC Biol. *7*, 12.

Nowack, E.C.M., Price, D.C., Bhattacharya, D., Singer, A., Melkonian, M., and Grossman, A.R. (2016). Gene transfers from diverse bacteria compensate for reductive genome evolution in the chromatophore of *Paulinella chromatophora*. Proc. Natl. Acad. Sci. USA *113*, 12214–12219.

Oborník, M., and Green, B.R. (2005). Mosaic origin of the heme biosynthesis pathway in photosynthetic eukaryotes. Mol. Biol. Evol. *22*, 2343–2353.

Ochman, H., Lawrence, J.G., and Groisman, E.A. (2000). Lateral gene transfer and the nature of bacterial innovation. Nature *405*, 299–304.

Otten, C., Brilli, M., Vollmer, W., Viollier, P.H., and Salje, J. (2018). Peptidoglycan in obligate intracellular bacteria. Mol. Microbiol. *107*, 142–163.

Polerecky, L., Adam, B., Milucka, J., Musat, N., Vagner, T., and Kuypers, M.M.M. (2012). Look@NanoSIMS—a tool for the analysis of nanoSIMS data in environmental microbiology. Environ. Microbiol. *14*, 1009–1023.

Priyam, A., Woodcroft, B.J., Rai, V., Munagala, A., Moghul, I., Ter, F., Gibbins, M.A., Moon, H., Leonard, G., Rumpf, W., et al. (2015). Sequenceserver: a modern graphical user interface for custom BLAST databases. bioRxiv. https://doi.org/10.1101/033142.

Quast, C., Pruesse, E., Yilmaz, P., Gerken, J., Schweer, T., Yarza, P., Peplies, J., and Glöckner, F.O. (2013). The SILVA ribosomal RNA gene database project: improved data processing and web-based tools. Nucleic Acids Res. *41*, D590–D596.

Richards, T.A., Leonard, G., Soanes, D.M., and Talbot, N.J. (2011). Gene transfer into the fungi. Fungal Biol. Rev. *25*, 98–110.

Robinson, T. (1976). D-amino acids in higher plants. Life Sci. *19*, 1097–1102.

Rognes, T., Flouri, T., Nichols, B., Quince, C., and Mahé, F. (2016). VSEARCH: a versatile open source tool for metagenomics. PeerJ *4*, e2584.

Sato, N., and Takano, H. (2017). Diverse origins of enzymes involved in the biosynthesis of chloroplast peptidoglycan. J. Plant Res. *130*, 635–645.

Schenk, H.E.A. (1970). Notizen: nachweis einer lysozymempfindlichen stützmembran der endocyanellen von Cyanophora paradoxa korschikoff. Z Naturforsch B *25*, 656–657.

Schleiff, E., and Soll, J. (2000). Travelling of proteins through membranes: translocation into chloroplasts. Planta *211*, 449–456.

Schloss, P.D., Westcott, S.L., Ryabin, T., Hall, J.R., Hartmann, M., Hollister, E.B., Lesniewski, R.A., Oakley, B.B., Parks, D.H., Robinson, C.J., et al. (2009). Introducing mothur: open-source, platform-independent, community-supported software for describing and comparing microbial communities. Appl. Environ. Microbiol. *75*, 7537–7541.

Schönknecht, G., Chen, W.-H., Ternes, C.M., Barbier, G.G., Shrestha, R.P., Stanke, M., Bräutigam, A., Baker, B.J., Banfield, J.F., Garavito, R.M., et al. (2013). Gene transfer from bacteria and archaea facilitated evolution of an extremophilic eukaryote. Science *339*, 1207–1210.

Sloan, D.B., Nakabachi, A., Richards, S., Qu, J., Murali, S.C., Gibbs, R.A., and Moran, N.A. (2014). Parallel histories of horizontal gene transfer facilitated extreme reduction of endosymbiont genomes in sap-feeding insects. Mol. Biol. Evol. *31*, 857–871.

Slot, J.C., and Rokas, A. (2011). Horizontal transfer of a large and highly toxic secondary metabolic gene cluster between fungi. Curr. Biol. *21*, 134–139.

Stairs, C.W., Eme, L., Muñoz-Gómez, S.A., Cohen, A., Dellaire, G., Shepherd, J.N., Fawcett, J.P., and Roger, A.J. (2018). Microbial eukaryotes have adapted to hypoxia by horizontal acquisitions of a gene involved in rhodoquinone biosynthesis. eLife *7*, e34292.

Thao, M.L., Gullan, P.J., and Baumann, P. (2002). Secondary (γ-Proteobacteria) endosymbionts infect the primary (β-Proteobacteria) endosymbionts of mealybugs multiple times and coevolve with their hosts. Appl. Environ. Microbiol. *68*, 3190–3197.

Timmis, J.N., Ayliffe, M.A., Huang, C.Y., and Martin, W. (2004). Endosymbiotic gene transfer: organelle genomes forge eukaryotic chromosomes. Nat. Rev. Genet. *5*, 123–135.

Typas, A., Banzhaf, M., Gross, C.A., and Vollmer, W. (2011). From the regulation of peptidoglycan synthesis to bacterial growth and morphology. Nat. Rev. Microbiol. *10*, 123–136.

van Baren, M.J., Bachy, C., Reistetter, E.N., Purvine, S.O., Grimwood, J., Sudek, S., Yu, H., Poirier, C., Deerinck, T.J., Kuo, A., et al. (2016). Evidence-based green algal genomics reveals marine diversity and ancestral characteristics of land plants. BMC Genomics *17*, 267.

van Teeseling, M.C.F., Mesman, R.J., Kuru, E., Espaillat, A., Cava, F., Brun, Y.V., VanNieuwenhze, M.S., Kartal, B., and van Niftrik, L. (2015). Anammox Planctomycetes have a peptidoglycan cell wall. Nat. Commun. *6*, 6878.

von Dohlen, C.D., Kohler, S., Alsop, S.T., and McManus, W.R. (2001). Mealybug beta-proteobacterial endosymbionts contain gamma-proteobacterial symbionts. Nature *412*, 433–436.

Wickham, H. (2009). ggplot2: Elegant Graphics for Data Analysis (Springer-Verlag).

Wolf, A.J., and Underhill, D.M. (2018). Peptidoglycan recognition by the innate immune system. Nat. Rev. Immunol. *18*, 243–254.

Yao, Z., Kahne, D., and Kishony, R. (2012). Distinct single-cell morphological dynamics under beta-lactam antibiotics. Mol. Cell *48*, 705–712.

Yarza, P., Richter, M., Peplies, J., Euzeby, J., Amann, R., Schleifer, K.-H., Ludwig, W., Glöckner, F.O., and Rosselló-Móra, R. (2008). The All-Species Living Tree project: a 16S rRNA-based phylogenetic tree of all sequenced type strains. Syst. Appl. Microbiol. *31*, 241–250.

STAR★METHODS

KEY RESOURCES TABLE

REAGENT or RESOURCE	SOURCE	IDENTIFIER
Antibodies		
Rabbit polyclonal anti-MurF	This paper; ProSci Incorporated	N/A
Goat polyclonal anti-rabbit IgG (H+L) Alexa Fluor 594	Abcam	Cat# 150084 RRID: AB_2734147
Normal goat serum	Vector Laboratories	Cat# S-1000 RRID: AB_2336615
Rabbit pre-immune serum	This paper; ProSci Incorporated	N/A
Chemicals, Peptides, and Recombinant Proteins		
Azide Alexa Fluor 488	Thermo Fisher Scientific	Cat# A10270
Cefsulodin	Research Products International	Cat# C52000
D-propargylglycine	Alfa Aesar	Cat# 15402639
Epon-Araldite resin kit	Electron Microscopy Sciences	Cat# 13940
Lysozyme	Thermo Fisher Scientific	Cat# 90082
MurF peptide (FVKSLENDYQKTKE)	This paper; ProSci Incorporated	N/A
Mutanolysin	Sigma-Aldrich	Cat# M9901
15N D-alanine	Sigma-Aldrich	Cat# 618527
15N L-alanine	Sigma-Aldrich	Cat# 332127
Paraplast Extra	Leica Biosystems	Cat# 39603002
Technovit 8100 resin kit	Electron Microscopy Sciences	Cat# 14654
Critical Commercial Assays		
Click-iT Reaction buffer kit	Thermo Fisher Scientific	Cat# C10269
DNeasy Blood and Tissue kit	QIAGEN	Cat# 69504
MiSeq Reagent Kit v2	Illumina	Cat# MS-102-2003
Nextera XT DNA library preparation kit	Illumina	Cat# FC-131-1096
Nextera XT indices	Illumina	Cat# FC-131-1002
Deposited Data		
Planococcus citri protein and nucleotide sequences	Priyam et al., 2015	https://blast.mealybug.org/
Tremblaya princeps protein and nucleotide sequences	NCBI	GenBank: CP002244
Moranella endobia protein and nucleotide sequences	NCBI	GenBank: CP002243
16S rRNA amplicon sequences	This paper	NCBI BioProject: PRJNA546070
SILVA rRNA database	Quast et al., 2013	https://www.arb-silva.de/
Experimental Models: Organisms/Strains		
Planococcus citri (Insecta: Hemiptera: Pseudococcidae)	University of Montana	N/A
Oligonucleotides		
536F (Prokaryotic 16S rDNA) (TCGTCGGCAGCGTCAG ATGTGTATAAGAGACAGCAGCMGCCGCGGTAATWC)	Holben et al., 2002	N/A
907R (Prokaryotic 16S rDNA) (GTCTCGTGGGCTCGGA GATGTGTATAAGAGACAGCCGTCAATTCMTTTRAGTTT)	Holben et al., 2002	N/A
Eub 338 (GCTGCCTCCCGTAGGAGT)	Fuchs et al., 2007	N/A
Gam42a (GCCTTCCCACATCGTTT)	Fuchs et al., 2007	N/A
Software and Algorithms		
Adobe Illustrator CC 2019	Adobe	https://www.adobe.com/
Byonic 3.3.9	Protein Metrics	https://www.proteinmetrics.com/products/byonic/
Effect Size Calculator for t test	Social Science Statistics	https://www.socscistatistics.com/effectsize/default3.aspx

(*Continued on next page*)

Continued

REAGENT or RESOURCE	SOURCE	IDENTIFIER
ggplot2 3.1.0	Wickham, 2009	https://ggplot2.tidyverse.org/
ImageJ 2.0.0	NIH	https://imagej.nih.gov/ij/
IMOD 4.9.10	Kremer et al., 1996	http://bio3d.colorado.edu/imod/
Look@nanoSIMS	Polerecky et al., 2012	http://nanosims.geo.uu.nl/nanosims-wiki/doku.php/nanosims:lans
MATLAB	MathWorks	https://www.mathworks.com/products/matlab.html
mothur 41.2	Schloss et al., 2009	https://www.mothur.org
RStudio 3.4.4	RStudio	https://www.rstudio.com/products/rstudio/
SerialEM	Mastronarde, 2005	http://bio3d.colorado.edu/SerialEM/
Trimmomatic 0.27	Bolger et al., 2014	http://www.usadellab.org/cms/index.php?page=trimmomatic
VSEARCH	Rognes et al., 2016	https://github.com/torognes/vsearch
ZEN Black	Zeiss	https://www.zeiss.com/microscopy/int/products/microscope-software/zen.html
Other		
Type A brass planchettes	Ted Pella Inc.	Cat# 39200
Type B brass planchettes	Ted Pella Inc.	Cat# 39201
Poly-L-lysine slides	Tekdon Incorporated	Cat# 10-61
AMPure XP beads	Beckman Coulter	Cat# A63880

LEAD CONTACT AND MATERIALS AVAILABILITY

Further information and requests for resources and reagents should be directed to and will be fulfilled by the Lead Contact, John McCutcheon (john.mccutcheon@umontana.edu). The reagents generated in this study are available from the Lead Contact with the following possible restrictions. Mealybug distribution may be restricted based on U.S.D.A. import/export regulations.

EXPERIMENTAL MODEL AND SUBJECT DETAILS

Mealybugs

Planococcus citri were reared on squash or sprouted potatoes at 25°C, 77% relative humidity, and 12 h light/dark cycles in a Percival 136LL incubator until use (Figure S1). Where bacteriomes were dissected, only second and third instar female insects were used. For the LC-MS/MS experiments, whole insects of all instars and both sex were used except winged fourth instar males as these no longer contain bacteriomes.

METHOD DETAILS

Gene annotation

A list of known PG-related genes was generated using published descriptions of the system (Husnik and McCutcheon, 2018; Husnik et al., 2013) (Table S1) along with more up-to-date literature on the PG pathways (primarily: Otten et al., 2018; Typas et al., 2011). One to six protein sequences for each gene were collected from different bacterial species on Uniprot and blasted against the genomes of *Candidatus* Tremblaya princeps (GenBank: CP002244), *Candidatus* Moranella endobia (GenBank: CP002243), and *Planococcus citri* (https://blast.mealybug.org; *Planococcus citri* Pcitri v1 proteins database) (Priyam et al., 2015). Top hits for any unannotated proteins were blasted using the NCBI non-redundant protein sequence database to confirm similarity to known versions of those proteins. Sequences in Table S1 for *P. citri* are from https://blast.mealybug.org.

Mealybug feeding and dissection

For detection of ^{15}N-labeled compounds by nanoSIMS, second and third instar mealybugs were moved to sprouted potatoes (Figure S1) that had been covered in 1 mL of 3.57 mg/mL of ^{15}N D-alanine or ^{15}N L-alanine (Sigma-Aldrich). The D-amino acids were dissolved in water and filtered through a 0.22 μM syringe filter. For fluorescent detection of D-alanine via click-chemistry and fluorescence microscopy, 3.57 mg/mL of D-propargylglycine (Alfa Aesar) was prepared and applied in the same manner as above. For both nanoSIMS and click chemistry experiments, the labeled compound treatments were reapplied every day for a

week with a 27-gauge needle and syringe and distributed gently with a paintbrush across the potato, focusing on sprouts or any locations near feeding mealybugs. The same process was used for the TEM antibiotic experiments using 100 μg/mL 0.22 μM-filtered cefsulodin (Research Products International) in water. One mL of water was added in the same manner as described above for all control animals. After seven days, the bacteriomes were dissected from *P. citri* in *Drosophila* Ringer's Solution (3 mM $CaCl_2 \cdot 2H_2O$, 182 mM KCl, 46 mM NaCl, 10 mM Tris base; adjusted to pH 7.2) and fixed as described in the following sections.

LC-MS/MS

Approximately 1500 *P. citri* individuals were collected whole and frozen at −80°C until use. The animals were suspended in 500 μL of chilled, filtered water, flash frozen in liquid nitrogen, and lysed using a 3 mm tungsten carbide bead in a Tissuelyser II (QIAGEN) for 3 min at 25 Hz, flipping the holders once and repeating. The lysates were dripped into 50 mL of boiling 6% SDS with constant stirring and boiled for 1 h; filtered water was added as it boiled off. The lysate was centrifuged at 130,000 x *g* for 1 h at room temperature (RT). The supernatant was decanted and the pellet resuspended with 50 mL filtered water and centrifuged as above for a total of 6 washes. The SDS-free pellet was resuspended in 25 mM NaH_2PO_4 (pH 5.5) and digested with 100 U of mutanolysin (Sigma-Aldrich) overnight at 37°C. The sample was dried under vacuum and resuspended in 50 μL 0.25 M $Na_2B_4O_7$ (pH 9.0). Terminal sugars were reduced by addition of $NaBH_4$ to a final concentration of 5 mg/mL and incubated at RT for 30 min. Reduction was terminated by addition of 15 μL H_3PO_4 (0.05% v/v). Reduced muropeptides were desalted by reverse-phase HPLC using water-formic acid 0.1% (v/v) and one-step elution with 25% acetonitrile (v/v)-formic acid 0.1% (v/v) gradient and analyzed by LC-MS/MS (Bern et al., 2017). Byonic version 3.3.9 was used to search LC-MS/MS data to identify PGmonomers (Bern et al., 2017).

16S rRNA sequencing

Total DNA was extracted with the DNeasy Blood and Tissue Kit (QIAGEN) from five pools of five *P. citri* (second and third instars) and from 30 μL of the total lysate (all instars) used in LC-MS/MS analysis. The V4 and V5 regions of the 16S rRNA gene were amplified from each pool of DNA using the primers 536F and 907R (Holben et al., 2002) and "Amplicon with overhang" cycle conditions (below).

Primer Name	Sequence
536F	**TCGTCGGCAGCGTCAGATGTGTATAAGAGACAGCAGCMGCCGCGGTAATWC**
907R	**GTCTCGTGGGCTCGGAGATGTGTATAAGAGACAGCCGTCAATTCMTTTRAGTTT**

Primer Name	Sequence
536F	TCGTCGGCAGCGTCAGATGTGTATAAGAGACAGCAGCMGCCGCGGTAATWC
907R	GTCTCGTGGGCTCGGAGATGTGTATAAGAGACAGCCGTCAATTCMTTTRAGTTT

Amplicon with overhang PCR conditions

Cycle Temp	Cycle Duration	Cycle Rounds
98°C	1 min	1
98°C	30 s	15
55°C	30 s	15
72°C	30 s	15
72°C	5 min	1

The PCR products were cleaned with AMPure XP beads (Beckman Coulter) and indexed using the Nextera XT Indicies DNA Library Preparation Kit (Illumina) per manufacturer's instructions and amplified with the "Index PCR" conditions (below).

Index PCR conditions

Cycle Temp	Cycle Duration	Cycle Rounds
95°C	3 min	1
95°C	30 s	12
55°C	30 s	12
72°C	30 s	12
72°C	5 min	1

The indexed amplicons were bead-cleaned as before and sequenced using a MiSeq v2 and related reagent kit (Illumina; University of Montana Genomics Core). MiSeq sequence data were quality-trimmed using Trimmomatic v.0.27 (ILLUMINACLIP:TruSeq3-PE.fa:2:30:10 LEADING:3 TRAILING:3 SLIDINGWINDOW:4:15 MINLEN:36) (Bolger et al., 2014), then processed using mothur v.41.2 (Schloss et al., 2009), following mothur's standard operating procedures for Illumina MiSeq data (Kozich et al., 2013). Briefly: Paired-end reads were combined into contigs, those with ambiguous base calls or lengths shorter than 410 bp were removed. Contigs were then aligned to the SILVA database (Release 132) (Quast et al., 2013; Yarza et al., 2008) of reference SSU rRNA genes. Sequences in poor alignments, as well as those containing homopolymers longer than 8 bp were removed. Sequences were then pre-clustered allowing up to four differences between sequences for merging. Chimeras were removed using the VSEARCH algorithm (Rognes et al., 2016). The resulting amplicons were then classified by comparing them to the SILVA database (release 132), using BLASTn (minimum query coverage: 90%) (Altschul et al., 1990). Summary data can be found in Table S2, reads are deposited at NCBI under BioProject ID: PRJNA546070.

FISH-nanoSIMS

Bacteriomes from ^{15}N-fed insects were fixed overnight at 4°C in 2% EM-grade paraformaldehyde (PFA) and embedded in Technovit 8100 (Electron Microscopy Sciences) following the manufacturer's protocol. Bacteriomes were located in blocks under a stereo-dissecting microscope and semi-thin sections between 1-2 μm were cut dry using an ultramicrotome with a glass knife. Sections were deposited in ~40 μL deionized water droplets on poly-L-lysine-coated wells of glass slides (Tekdon Incorporated). Slides were screened for sections free from folds or tears for FISH reactions. FISH reactions were conducted under standard conditions (Fuchs et al., 2007). Briefly, FISH probes (below) targeting gammaproteobacterial 23S rRNA (Gam42a) (Fuchs et al., 2007) and general eubacterial 16S rRNA sequences (Eub 338 mix) (Fuchs et al., 2007) were combined in hybridization buffer (900 mM NaCl, 20 mM Tris-HCl, 0.01% SDS, pH 7.5) containing 35% formamide and 40 μL was spotted onto each section and hybridized in 50 mL Falcon tubes used as humidity chambers for 3 h. For the D-alanine samples (Figure 3A), Gam42a and Eub 338 mix were labeled with Cy3 and Alexa 647, respectively. For the L-alanine control (Figure 3F) the fluorophores were switched. Following the FISH reactions, samples were briefly air-dried and immediately covered with ~10 μL of mounting medium containing 4.5 μg/mL DAPI in Citifluor. Maps of FISHed sections were made on a Zeiss Elyra S.1 system.

FISH Probes	Sequence
Gam42a	GCCTTCCCACATCGTTT
Eub 338	GCTGCCTCCCGTAGGAGT

Note: *Tremblaya* 23S rRNA has significant mismatches with the traditional betaproteobacterial probe Bet42a, so *Tremblaya* cytoplasm was identified as the presence of Eub 338 mix signal, and lack of Gam42a signal. After the FISH imaging, coverslips were removed gently in a Petri dish filled with deionized water. Deionized water was gently poured over the slide for two min to remove mounting medium, with care taken to not dislodge sections by direct flow. Slides were air-dried, scored with a diamond scribe, and broken and filed to fit into nanoSIMS sample holders. Fragments were gold coated with a Cressington sputter coater (40 nm gold thickness). NanoSIMS analyses were carried out using a Cameca NanoSIMS 50L (Cameca). Fluorescence-microscopy mapped sample regions were identified using the nanoSIMS CCD camera. Samples were pre-sputtered with the Cs^+ ion beam (D1 = 1, 1 nA) until the $^{12}C^{15}N–$ ion counts stabilized. Bacteriomes were imaged using a ~1 pA primary Cs^+ ion beam current (D1 = 3), a raster size of 10 × 10 μm at 256 × 256 pixel resolution or 20 × 20 μm at 512 × 512 pixel resolution. Masses ($^{12}C^{14}N–$, $^{12}C^{15}N–$, ^{31}P, ^{32}S) were collected in parallel using electron multipliers with a dwell time of 12-48 ms/pixel. Mass calibration was performed every ~1 h for all masses. NanoSIMS .im data files were initially processed with the look@nanoSIMS package (Polerecky et al., 2012) in MATLAB (MathWorks) for frame alignment and raw data export. Large bacteriome images were created by manually stitching together tiled analyses. Box trace data were generated by exporting raw data as images and using the Plot Profile function in ImageJ to calculate average fractional abundance values along transects across the *Moranella* cell wall.

Cu-click chemistry

Whole bacteriomes were fixed in 2% PFA in 0.1 M cacodylate and 5% sucrose solution (cacodylate buffer) then rehydrated with PBS for 15 min at RT followed by permeabilization with 0.5% Triton X-100 in PBS for 15 min at RT. The bacteriomes were washed with 2% BSA in PBS (pH 7.35) and then resuspended in 500 μL of Click-iT reaction cocktail (Thermo Fisher) according to the manufacturer's protocol with 2.5 μM Alexafluor 488-azide (Thermo Fisher) and incubated for 1 h at RT protected from light followed by a 5 min wash in 2% BSA in PBS and a final resuspension in ProLong Gold Antifade mountant with DAPI (Invitrogen). The tissue was incubated at 4°C overnight, protected from light after which the bacteriomes were pipetted onto a clean glass slide and a glass coverslip was carefully placed on top. Thirty to fifty Z stacks were acquired for each bacteriome using a Zeiss 880 laser scanning confocal microscope at 63X magnification (63X objective, type: Plan-Apochromat, aperture: 1.4, immersion: oil) and ZEN Black software (Zeiss). Z stacks were

analyzed using ImageJ (Version 2.0.0). Background was subtracted from all channels using a 50-pixel rolling ball radius; a representative image was created using the Z-project and Max Intensity options for four consecutive slices of a single Z stack.

TEM and dual-axis tomography

Bacteriomes used for TEM were fixed in 3% EM-grade glutaraldehyde and 1% EM-grade PFA in cacodylate buffer on ice and shipped overnight where they were immediately rinsed with fresh cacodylate buffer and placed into Type A brass planchettes (Ted Pella, Inc.) prefilled with 10% Ficoll in cacodylate buffer. Nodes were covered with the flat side of a Type B brass planchette and the samples were rapidly frozen with a HPM-010 high-pressure freezing machine (Leica Microsystems). The vitrified samples were transferred under liquid nitrogen to cryotubes containing a frozen solution of 2.5% osmium tetroxide, 0.05% uranyl acetate in acetone. Tubes were loaded into an AFS-2 freeze-substitution machine (Leica Microsystems) and processed at −90°C for 72 h, warmed over 12 h to −20°C, held at that temperature for 8 h, then warmed to 4°C for 1 h. The fixative was removed and the samples rinsed 4X with cold acetone following which they were infiltrated with Epon-Araldite resin (Electron Microscopy Sciences) over 48 h. Bacteriomes were embedded on Teflon-coated glass microscope slides using Secure-Seal imaging spacers (Sigma-Aldrich) and covered with Thermanox coverslips (Electron Microscopy Sciences). Resin was polymerized at 60°C for 48 h. Embedded bacteriomes from age-matched insects were observed with a stereo-dissecting microscope to ascertain and select well-preserved samples. Bacteriomes were extracted with a microsurgical scalpel and glued to the tips of plastic sectioning stubs. Semi-thick (400 nm) serial sections were cut with a UC6 ultramicrotome (Leica Microsystems) using a diamond knife (Diatome, Ltd.). Sections were placed on Formvar-coated copper-rhodium slot grids (Electron Microscopy Sciences) and stained with 3% uranyl acetate and lead citrate. Ten nm gold beads were placed on both surfaces of the grid to serve as fiducial markers for subsequent image alignment. Sections were placed in a dual-axis tomography holder (Model 2040, E.A. Fischione Instruments) and imaged with a Tecnai TF30ST-FEG transmission electron microscope (300 KeV; Thermo Fisher) equipped with a 2k x 2k CCD camera (XP1000; Gatan, Inc.). Tomographic tilt-series and large-area montaged overviews were acquired automatically using the SerialEM software package (Mastronarde, 2005). For tomography, samples were tilted ± 64° and images collected at 1° intervals. The grid was then rotated 90° and a similar series taken about the orthogonal axis. Tomographic data were calculated and analyzed using the IMOD software package (Kremer et al., 1996).

Immunohistochemistry

Whole third instar insects were gently perforated with a dissection pin and fixed in 4% PFA in PBS for 1.5 h at RT, washed in PBS 3X for 10 min, and transferred to 30% EtOH for 10 min followed by fresh 30% EtOH overnight at 4°C. The following day, samples were dehydrated through a series of EtOH: 50%, 70%, 80%, 90%, 95%, (2X 10 min each at RT). Samples were transferred to 100% EtOH (1 h at RT), methyl salicylate (3X 20 min at RT) and Paraplast Extra (2X 20 min, 1X 45 min at 56°C; Leica Biosystems) and then embedded in paraffin. Tissue was sectioned at 5 μm and the location of bacteriome was mapped by hematoxylin (Cancer Diagnostics) and eosin (Cancer Diagnostics) staining in a subset of sections. A custom polyclonal antibody was generated (ProSci Incorporated) to a peptide sequence (FVKSLENDYQKTKE) from the *P. citri murF* gene (accession: AGR65718) that was predicted to be surface exposed. Antibody response to the immunizing peptide was confirmed by ELISA by ProSci Incorporated. For staining, sections were deparaffinized and rehydrated in distilled water. The PG membrane was permeabilized by incubating sections in 2 mg/mL lysozyme (Thermo Fisher Scientific) in dH_2O for 30 min at 37°C followed by two PBS washes, and then incubated in 0.1% Triton X-100 in PBS for 5 min at RT (Cimino et al., 2006). Sections were washed 2X in PBS and then treated for heat-induced antigen retrieval by boiling for 10 min in 0.01 M citrate (pH 6.0) and returned to RT for 30 min. The tissue was then washed in PBS, blocked in 4% normal goat serum (Vector Laboratories) for 20 min at RT, and incubated in a 1:50 dilution of primary antibody in 0.05% BSA in PBS for 1 h at RT then overnight at 4°C. Negative controls were incubated with either no primary antibody or with pre-immune serum from the rabbit used to produce the primary antibody (ProSci Incorporated). The following day, sections were washed 3X in PBS. Primary antibody was detected by incubation with Alexa Fluor 594 Goat anti-rabbit IgG secondary antibody (1:400 in PBS; Abcam) for 1.5 h at RT. DNA was labeled with 40 μg/mL Hoechst 33342 Solution (Sigma-Aldrich) in PBS for 10 min at RT. Sections were washed 3X in PBS and then mounted using FluorSave reagent (EMD Millipore). All imaging was done using identical settings as described for Cu-click chemistry. Linear contrast stretching was applied equally to antibody stained tissue and matching controls using ImageJ.

QUANTIFICATION AND STATISTICAL ANALYSIS

Membrane measurements

Five TEM images from the bacteriomes of each of four, age-matched, *P. citri* (two control and two cefsulodin-treated) for a total of 20 images were analyzed for differences in the periplasm width of *Tremblaya* and *Moranella*. Twenty measurements of the distance between the outside of the outermost membrane and the inside of the innermost membrane for one to three *Tremblaya* (n = 200) and *Moranella* (n = 400) cells as well as the for the innermost and middle membrane of *Tremblaya* (n = 200) in each image were taken using the IMOD software package (Kremer et al., 1996) (Table S3, related to Figure 4). Data were visualized using ggplot2 (Wickham, 2009)

in RStudio. The boxplots (Figure 4A) show the mean ± SEM (also listed in the Results) with overlaid jitter plot of all data points; p values are reported above each comparison and total n are listed here as well as in the legend. The control and cefsulodin-treated animals were compared using a student's two-sided t test in RStudio. Effect size calculations were performed using the Effect Size Calculator for t-Test (https://www.socscistatistics.com/effectsize/default3.aspx).

DATA AND CODE AVAILABILITY

16S rRNA amplicon sequences have been deposited in NCBI under BioProject ID: PRJNA546070. All membrane measurements presented in Figure 4 are included in this manuscript as Table S3.

Cell

Figure S1. Representative Setup for Rearing and Feeding Experiments Involving *P. citri*, Related to Figures 2, 3, 4, and 5

Mealybugs (yellow arrows) were allowed to feed and reproduce on sprouted potatoes. Where treatments were applied, potatoes (often focusing on the sprouts) were covered and/or injected with 1 mL of the given treatment (modified D- or L-ala, cefsulodin, or water). Mealybugs were carefully placed on the potato with a paintbrush and allowed to eat *ad libitum*. Treatments were repeated each day for one week.